The Meteoritical Society

Meteoritics & Planetary Science 50, Nr 6, 1032–1049 (2015)
doi: 10.1111/maps.12452

Refractory inclusions in the pristine carbonaceous chondrites DOM 08004 and DOM 08006

Steven B. SIMON[1*] and Lawrence GROSSMAN[1,2]

[1]Department of the Geophysical Sciences, The University of Chicago, 5734 S. Ellis Ave., Chicago, Illinois 60637, USA
[2]The Enrico Fermi Institute, The University of Chicago, 5640 S. Ellis Ave., Chicago, Illinois 60637, USA
[*]Corresponding author. E-mail: sbs8@uchicago.edu

(Received 19 September 2014; revision accepted 03 March 2015)

Abstract–The Antarctic carbonaceous chondrites DOM 08004 and DOM 08006 have been paired and classified as CO3.0s. There is some uncertainty as to whether they should be paired and whether they are best classified as CO chondrites, but they provide an opportunity for the study of refractory inclusions that have not been modified by parent body processes. In this work, refractory inclusions in thin sections of DOM 08004 and 08006 are studied and compared with inclusions in ALHA77307 (CO3.0) and Acfer 094 (C3.0, ungrouped). Results show that the DOM samples have refractory inclusion populations that are similar to each other but not typical of CO3 chondrites; main differences are that the DOM samples are slightly richer in inclusions in general and, more specifically, in the proportions of grossite-bearing inclusions. In DOM 08004 and DOM 08006, 12.4% and 6.6%, respectively, of the inclusions are grossite-bearing. This is higher than the proportion found in Acfer 094 (5.2%), whereas none were found in ALHA77307. Like those in Acfer 094, DOM inclusions are small (mostly <100 μm across) and fine-grained, and thin rims of aluminous diopside±melilite are very common. Also like Acfer 094, most phases in the DOM inclusions have FeO contents higher than expected for primary refractory phases. In addition to typical inclusions, some unusual ones were found in DOM 08004, including a perovskite-rich one with a rare, recently reported Sc-, Al-oxide and davisite; a very grossite-rich inclusion with a small, hibonite-rich core enclosed in a grossite mantle; and a relict, grossite-rich inclusion enclosed in an Al-rich chondrule. The CAI populations in the DOM samples are similar to each other and, based on grossite abundances, FeO enrichments and occurrences of rims are more Acfer 094-like than CO3-like. An earlier history on an FeO-rich parent was previously favored over nebular equilibria or in situ reactions to account for FeO enrichments in CAIs in the otherwise pristine chondrite Acfer 094, and a similar history is indicated for the DOM CAIs. Acfer 094, DOM 08004 and 08006 might best be classified as a new subgroup of CO3 chondrites.

INTRODUCTION

Pristine carbonaceous chondrites are of great interest because they contain nebular and presolar materials that have undergone little or no modification by planetary processes in meteoritic parent bodies. The CO (Ornans-type) carbonaceous chondrites exhibit a range of metamorphic grade from 3.00 (pristine) to 3.8 (nearly equilibrated). Among these samples, with increasing grade, contents of presolar grains decrease and the extent of alteration of refractory inclusions increases. Several carbonaceous chondrites, including the Antarctic samples ALHA77307 and DOM 08006, have been classified as CO3.00 (Davidson et al. 2014). They have similar matrices to each other, consisting of highly unequilibrated assemblages with high amorphous silicate and presolar grain contents, and ferroan olivine with high Cr_2O_3 contents, indicating little metamorphism-induced exsolution has occurred (Grossman and Brearley 2005; Davidson et al. 2014).

While some pristine meteorites fall into recognized groups, others do not. Study of the Ca-, Al-rich refractory inclusions (CAIs) in them can provide insights into nebular processes and can be used to classify and compare similar meteorites. One of the most important samples in our collections, and one of the most intensely studied is the ungrouped C3 Acfer 094. It has a distinctive refractory inclusion population (Krot et al. 2004; Simon and Grossman 2011) and high contents of presolar silicate and oxide grains (Nguyen et al. 2007), which is an indicator of pristinity because they are easily destroyed. In a study of Fe-Ni metal in primitive chondrites, Kimura et al. (2008) found Acfer 094 to be even more primitive than ALHA77307, assigning a grade of 3.00 to the former and 3.03 to the latter.

DOM 08004 also is a C3 chondrite. It has been paired with DOM 08006, but some differences have been observed that call this pairing into question. For example, Alexander et al. (2014) reported $\delta^{13}C$ values of −4.2 and −5.0‰ for DOM 08006 and −11.3‰ for DOM 08004. Another basis for comparison of these samples is their refractory inclusion populations. We have studied the refractory inclusions found in thin sections of DOM 08004 and DOM 08006 in order to (1) investigate inclusions free of metamorphic overprints; (2) look for new type of inclusions; (3) see if the CAI populations support pairing of the specimens; and (4) compare them with the CAI populations in ALHA77307 and Acfer 094 (Simon and Grossman 2011), to see whether either or both of the DOM samples should be classified as CO chondrites or if they are actually more similar to Acfer 094. In a previous study of the refractory inclusions in Acfer 094 (Simon and Grossman 2011), we found that almost every phase in almost every inclusion analyzed was enriched in FeO compared to what would be expected for unaltered CAIs from the solar nebula. Since this enrichment was not due to in situ parent-body processes, it must be a feature the inclusions acquired prior to the accretion of Acfer 094. This distinctive feature will be helpful in identifying Acfer 094-like chondrites in this and future studies. Preliminary results of this work were reported by Simon and Grossman (2014).

ANALYTICAL METHODS

Using methods similar to those of Simon and Grossman (2011), polished thin sections of DOM 08004, DOM 08006, and ALHA77307 were searched for CAIs by simultaneous collection of backscattered electron images and Al Kα X-ray maps with a JEOL JSM-5800 LV scanning electron microscope operated at 90× and 15 kV. All Al-rich objects were investigated and their constituent phases identified with an Oxford/Link ISIS-300 energy-dispersive X-ray analysis system. Quantitative wavelength-dispersive analyses of phases in inclusions selected for detailed study were obtained with a fully automated Cameca SX-50 electron microprobe operated at 15 kV operated with beam currents of 25–40 nA and equal peak and background counting times that ranged from 10 s (Na, Mg, Al) to 30 s. Data were reduced using the modified ZAF correction procedure PAP (Pouchou and Pichoir 1984).

RESULTS

Abundances and Populations of Refractory Inclusions

In DOM 08004, 218 inclusions were found in 140 mm^2, yielding an inclusion density of 1.6 inclusions per mm^2. The section of DOM 08006 available to us contained much less material (22.5 mm^2) than the other sections studied and only 30 inclusions were found in it, so the statistics may not be representative, but that section averaged 1.4 inclusions per mm^2, a result very close to that for 08004. In comparison, searches using the same method in the same laboratory yielded 0.9 inclusions mm^{-2} in 114 mm^2 of ALHA77307 and 3.2 inclusions mm^{-2} in 89.1 mm^2 of Acfer 094. Thus, per unit of surface area, Acfer 094 is richest in refractory inclusions, ALHA77307 poorest, with DOM 08006 and 08004 intermediate between them. Carbonaceous chondrites are known to be heterogeneous, and in other studies of ALHA77307, Russell et al. (1998) found just 0.3 inclusions mm^{-2} while Han (2014) found 1.5 and 1.9 per mm^2 in two sections of the sample. Studies of other low-grade CO3s yielded results within this range. Kojima et al. (1995) found 1.1 per mm^2 in Y-81020, a CO3.0, and Davis (1985) found 0.6 per mm^2 in Ornans, which has a metamorphic grade of 3.3.

Inclusions are classified herein simply on the basis of the mineral assemblages observed, without genetic interpretations based on textures or proportions of phases except for the identification of rims, which are not considered as part of the primary phase assemblages. Many inclusions are small (typically <100 μm across), unrimmed fragments and it is not known how representative they are of their parent objects either texturally or modally.

Some first-order similarities between CAI populations in the DOM samples and those in Acfer 094 and ALHA are noted when inclusions are grouped into the following six categories of primary mineral assemblages: melilite (mel)+spinel (sp)+perovskite (pv); mel+sp; sp+pv; sp; hibonite-bearing; and grossite-bearing. These groups together account for 65.4–96.5% of the numbers of inclusions found in the samples

Table 1. Modal abundances (% of total found, i.e., *n*) of refractory inclusions in the present samples, compared to those in Acfer 094.

	DOM 08004	DOM 08006	ALHA 77307	Acfer 094
Grossite-bearing	12.4	6.6	0	5.2
Hibonite-bearing	11.0	16.5	17.3	11.9
Spinel	4.1	6.7	5.8	9.7
Sp+Pv	12.4	26.7	23.1	16.3
Mel+Sp	12.4	13.3	8.6	8.6
Mel+Sp+Pv	21.1	26.7	18.3	13.7
Other[a]	26.6	3.5	26.9	34.6
n	218	30	104	289

[a]Mainly monomineralic melilite fragments, melilite+perovskite inclusions, pyroxene-bearing assemblages, and anorthite-bearing assemblages.

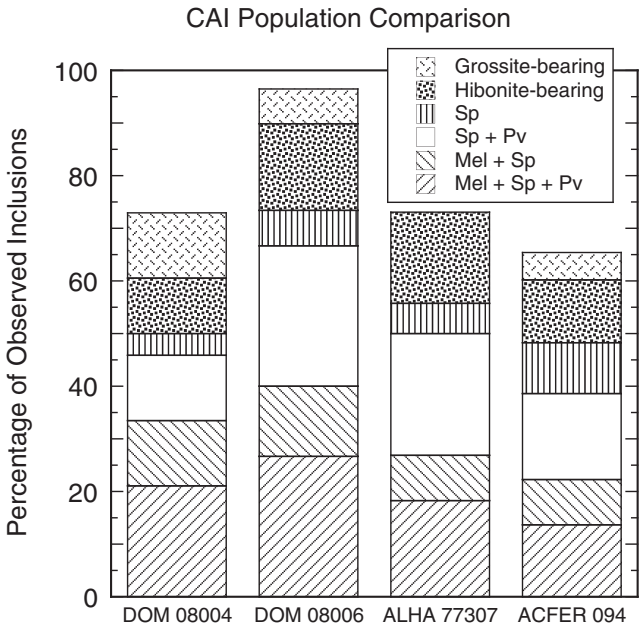

Fig. 1. Abundances of types of refractory inclusions by mineral assemblage. Percentages in Acfer 094 are from Simon and Grossman (2011). Sp = spinel; Pv = perovskite; Mel = melilite. *n* = 218 for DOM 08004; 30 for DOM 08006; 104 for ALHA77307; and 289 for Acfer 094.

(Table 1). The remainder mainly comprises monomineralic melilite fragments, mel+pv inclusions, pyroxene-bearing assemblages (especially in ALHA77307), and anorthite-bearing assemblages. The individual abundances of the six dominant assemblages are illustrated in Fig. 1, which shows that 50–73% of the inclusions in all samples studied have sp±mel±pv. In 08004, inclusions consisting of mel+sp and sp+pv are equally abundant (12.4%), about half as common as mel+sp+pv inclusions (21.1%), and more abundant than monomineralic spinel inclusions (4.1%). In 08006, mel+sp+pv and sp+pv inclusions are equally abundant (26.7%), twice as abundant as mel+sp (13.3%), and four times as common as monomineralic spinel (6.7%).

Proportions of hibonite-bearing (±grossite) inclusions range from 11.0% (08004) to 17.3% (77307) of the total found. Abundances of grossite-bearing (±hibonite) inclusions are zero in ALHA77307, 5.2% in Acfer 094, 6.6% in DOM 08006, and 12.4% in DOM 08004. Han (2014) found 333 CAIs in ALHA77307 but no grossite-bearing ones. In their study of refractory inclusions in CO3 chondrites, Russell et al. (1998) also did not find any grossite-bearing CAIs in ALHA77307, nor in any of the other nine CO3s they studied, although they reported two grossite-bearing CAIs in the Colony CO3.0 chondrite that had previously been described by Greenwood et al. (1992). Davis (1985) did not find any grossite-bearing inclusions among the 44 CAIs he found in a section of Ornans. Kojima et al. (1995) found two in their section of Y-81020 and none in the other two CO3s they studied. The present results, along with these previous studies, indicate that grossite-bearing inclusions are typically much rarer in CO3 chondrites than in Acfer 094 or the DOM samples considered here.

Petrography of Refractory Inclusions

Spinel±Melilite±Perovskite Assemblages

These inclusions are typically ~50 μm across and fine-grained (≤10 μm). A wide range of modal melilite/spinel ratios is observed. Melilite is largely unaltered. Thin, outer rims of aluminous diopside are common, especially on inclusions in the DOM and Acfer samples. Inclusions with one of the typical textures, consisting of fine, anhedral grains of spinel and perovskite enclosed in melilite, are shown in Figs. 2a–c. Objects like these have been previously described from CO3s (Russell et al. 1998) and Acfer 094 (Krot et al. 2004), and they have been called type A inclusions based on the similarity of their mineralogy to that typical of the larger, coarser, and more complete compact type A inclusions found in CV chondrites (Simon et al. 1999).

Inclusions consisting of nodules with grains of spinel±perovskite with melilite rims also occur (Figs. 3a–c). While these may be considered to have "fluffy" textures, most are not as melilite-rich as coarse-grained "fluffy" Type A inclusions found in CV chondrites (MacPherson and Grossman 1984). Compaction of nodular inclusions (e.g., Fig. 3a) could have led to the formation of the two very similar-looking inclusions from DOM 08004 and Acfer 094 shown in Figs. 3d and 3e. Small inclusions consisting of

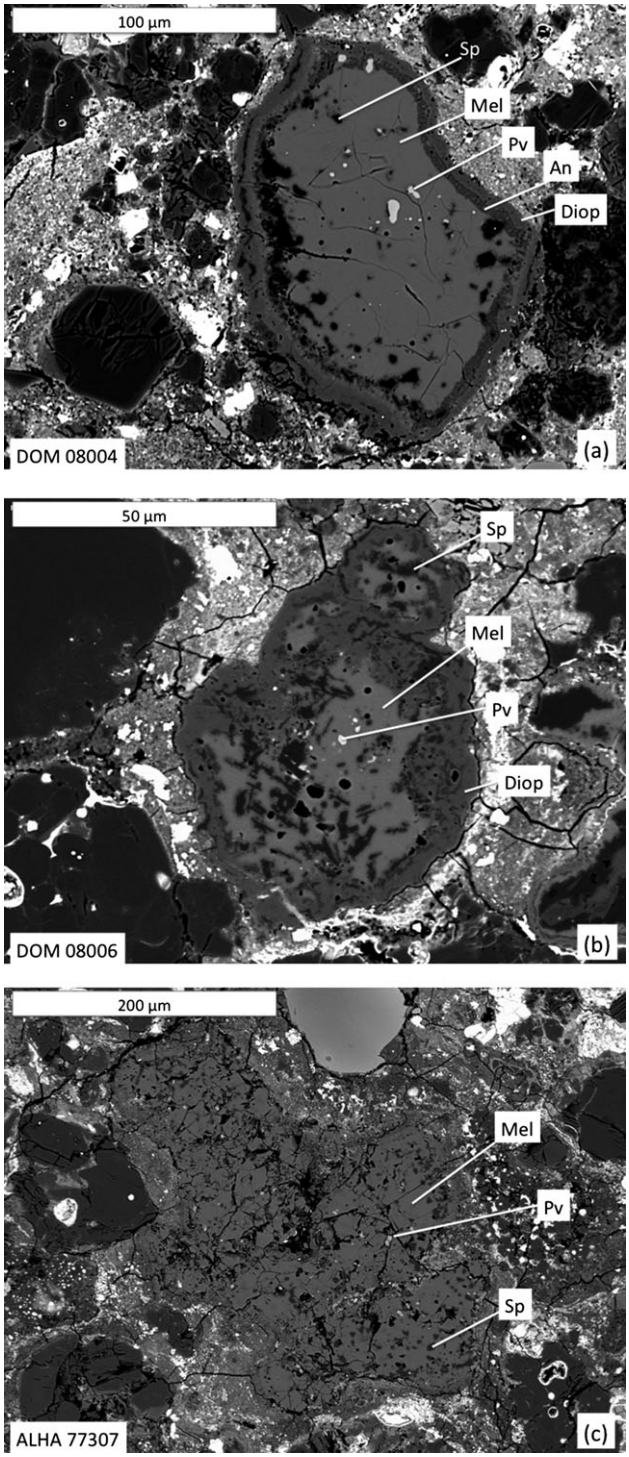

Fig. 2. Backscattered electron images of compact inclusions with spinel and perovskite enclosed in melilite. a) DOM 08004 inclusion 26-2. b) DOM 08006 inclusion 1-2. c) ALHA77307 inclusion 60-1. Abbreviations as in Fig. 1, plus An = anorthite; Diop = diopside.

spinel grains enclosing perovskite might have been derived by fragmentation from nodular inclusions like those shown in Fig. 3.

Hibonite-Bearing, Grossite-Bearing, and Hibonite-Grossite-Bearing Inclusions

Hibonite-Bearing, Grossite-Free

Of the 16 DOM 08004 inclusions that are in this category, 14 consist of hibonite+spinel+perovskite± melilite. Most are small fragments of hibonite-, spinel-rich spherules or are rounded hibonite grains with spinel and melilite±pyroxene rims (e.g., Fig. 4a). The other two are a porous hibonite-spinel spherule fragment with a trace amount of Ti-bearing pyroxene and a diopside rim, as might be found in a CM chondrite; and a hibonite-pyroxene spherule fragment, like those found in CM and CO chondrites (Tomeoka et al. 1992; Russell et al. 1998; Simon et al. 1998). An unusual inclusion, with three texturally distinct areas, is shown in Figs. 4b and 4c. It consists of hibonite, spinel, perovskite, and melilite grains that are mostly 5–10 µm across. Part of the inclusion is compact, part is loosely packed, and part is very perovskite-rich compared to the rest of the inclusion. This could be a fragment of a compound inclusion like the one from Acfer 094 described by Simon and Grossman (2011).

In addition to one monomineralic occurrence of hibonite, three grossite-free, hibonite-bearing inclusion fragments were found in DOM 08006, with the assemblages: hibonite+spinel+perovskite; hibonite+perovskite+melilite+Ti-bearing pyroxene; and hibonite+pyroxene.

Grossite-Bearing, Hibonite-Free

Nineteen inclusions found in DOM 08004 are grossite-bearing and hibonite-free. The most common assemblage is grossite with melilite+spinel+perovskite (8), followed by melilite+perovskite (5); spinel+perovskite (3), and one each with melilite+spinel; just spinel; and just perovskite. Examples are shown in Fig. 5. In most of the occurrences in DOM 08004, grossite has fine stringers of an Fe-, Na-bearing oxide lining cavities and filling cracks (e.g., Figs. 5a and 6) even where coexisting phases show no signs of alteration. This phase appears to contain Al_2O_3 as well but its contents of this oxide cannot be determined with confidence due to the thinness of the veins and the high Al_2O_3 content of the adjacent grossite. In one occurrence (Fig. 5b), where the grossite does not exhibit this feature, however, the perovskite has been partially altered to an Fe-Ti oxide identified from electron probe analyses as ulvöspinel, Fe_2TiO_4.

One hibonite-free, grossite-bearing object was found in DOM 08006. It consists of grossite, melilite, spinel, and perovskite, the most common grossite-bearing assemblage found in DOM 08004.

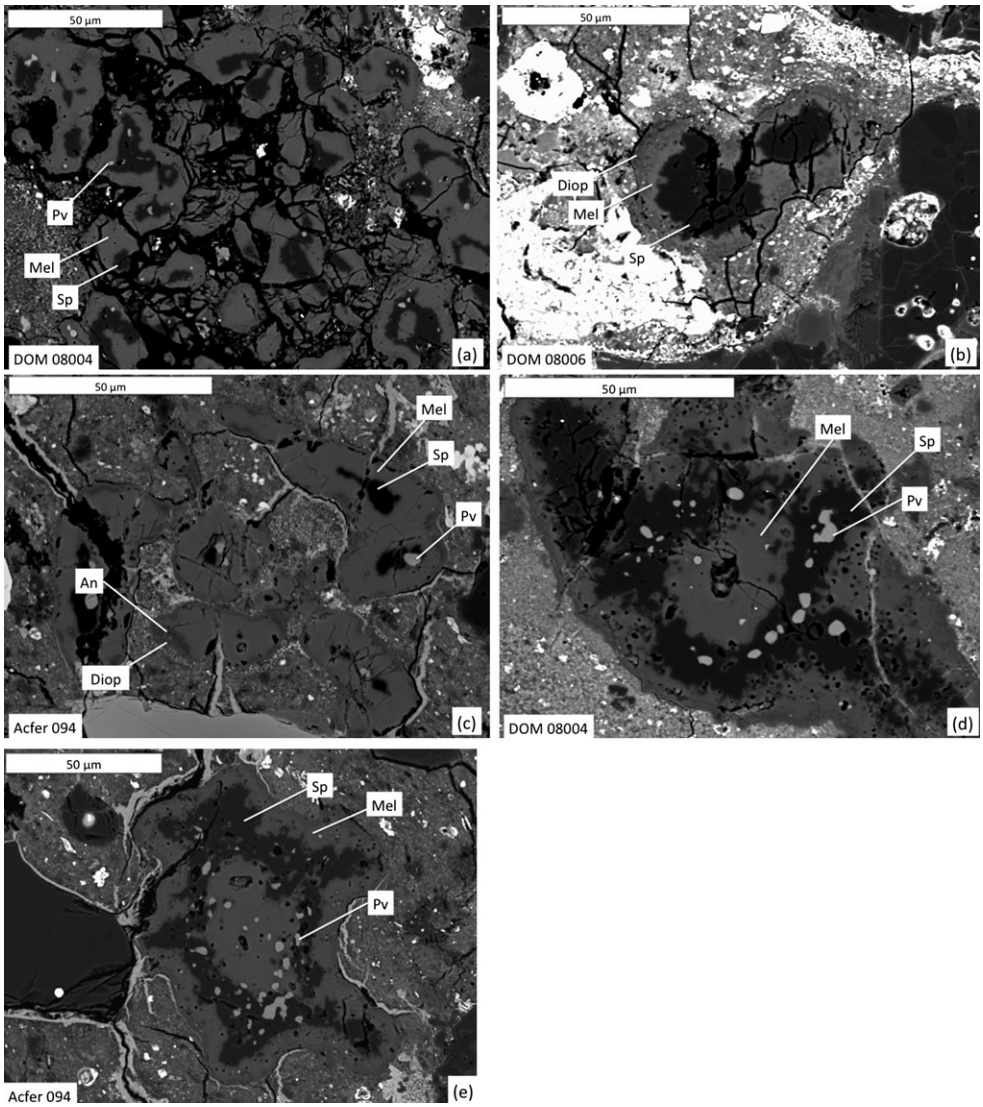

Fig. 3. Backscattered electron images of nodular melilite+spinel+perovskite inclusions. Abbreviations as in Fig. 2. a) DOM 08004 inclusion 84-1. b) DOM 08006 inclusion 1-4. c) Acfer 094 inclusion 28-4. d) DOM 08004 inclusion 32-1. e) Acfer 094 inclusion 28-1, very similar to the DOM 08004 inclusion shown in (d).

Hibonite-, Grossite-Bearing

Eight inclusions found in DOM 08004 contain both hibonite and grossite, several of which have unusual features and are worthy of special mention. One is 16-1 (Figs. 6a and 6b), a relatively large (200 μm across), zoned, very grossite-rich inclusion. It has a small core of hibonite enclosed in a thick mantle of grossite, enclosed in rim layers of gehlenitic melilite and pyroxene. Perovskite is enclosed in grossite throughout and it also occurs with spinel near the grossite-melilite contact. FeO-rich alteration products occur in pockets and in thin veins in grossite, hibonite, and, to a much lesser extent, in the pyroxene rim. Also noteworthy is 51-1, a grossite-hibonite-perovskite-spinel-melilite-anorthite-bearing object enclosed in an Al-rich chondrule fragment consisting of anorthite, enstatite, Al-diopside, and Fe,Ni metal (Fig. 6c). A trace amount of a fine, SiO_2-rich phase, not visible in Fig. 6, occurs interstitial to anorthite and enstatite laths in an assemblage similar to the crystalline mesostasis found in an Al-rich chondrule in Acfer 094 by Krot et al. (2004). The refractory inclusion (Fig. 6d) consists of pockets of grossite and melilite enclosed in spinel, with hibonite occurring between spinel and melilite, between spinel and grossite, and between melilite and grossite. Anhedral perovskite grains ~5 μm across are enclosed in spinel, melilite, and in grossite, and some hibonite laths extend into and even through perovskite grains. Accessory anorthite occurs enclosed in melilite and in spinel. As in other occurrences in DOM 08004, grossite in 51-1 has

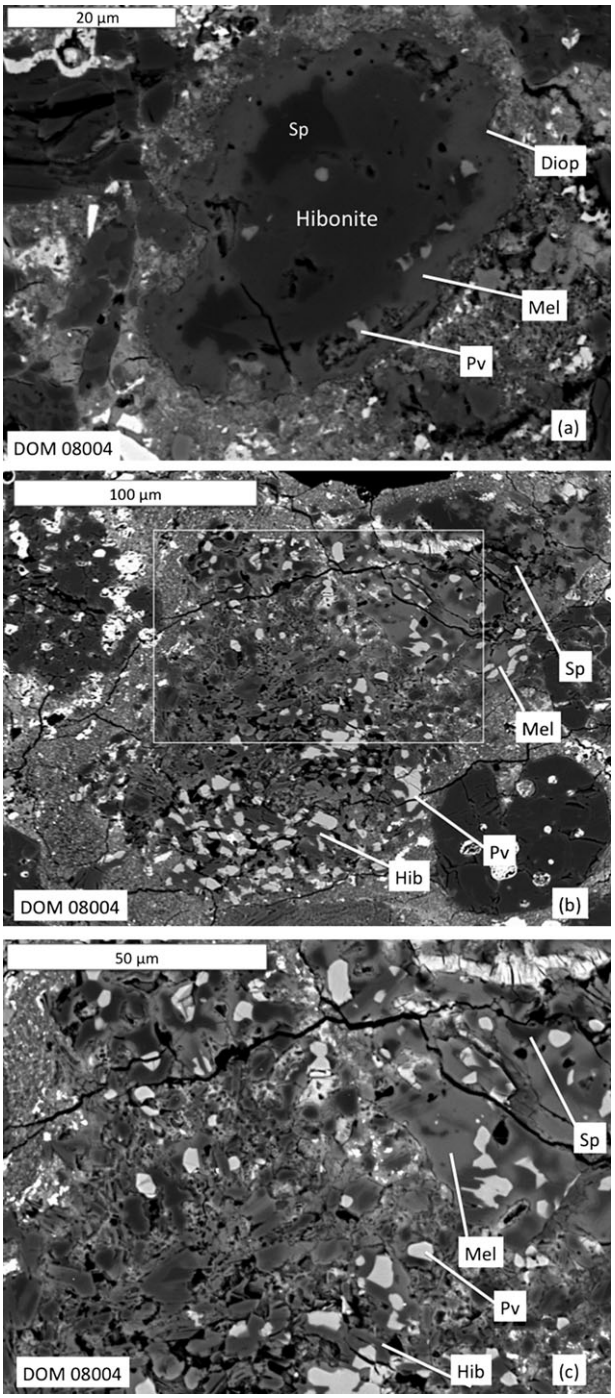

Fig. 4. Backscattered electron images of hibonite-bearing, grossite-free inclusions. Abbreviations as in Fig. 2, plus Hib = hibonite. a) Hibonite-spinel-perovskite inclusion 29-3 from DOM 08004. Melilite+aluminous-diopside rim. b) Inclusion with a heterogeneous texture in DOM 08004. Upper part is compact and melilite-rich compared to the middle part, which is relatively porous and hibonite-rich, and the lowermost part, which is porous and perovskite-rich. Outlined area is shown in (c), in which the compact portion is seen at the upper right, the relatively porous, hibonite-rich region at lower left.

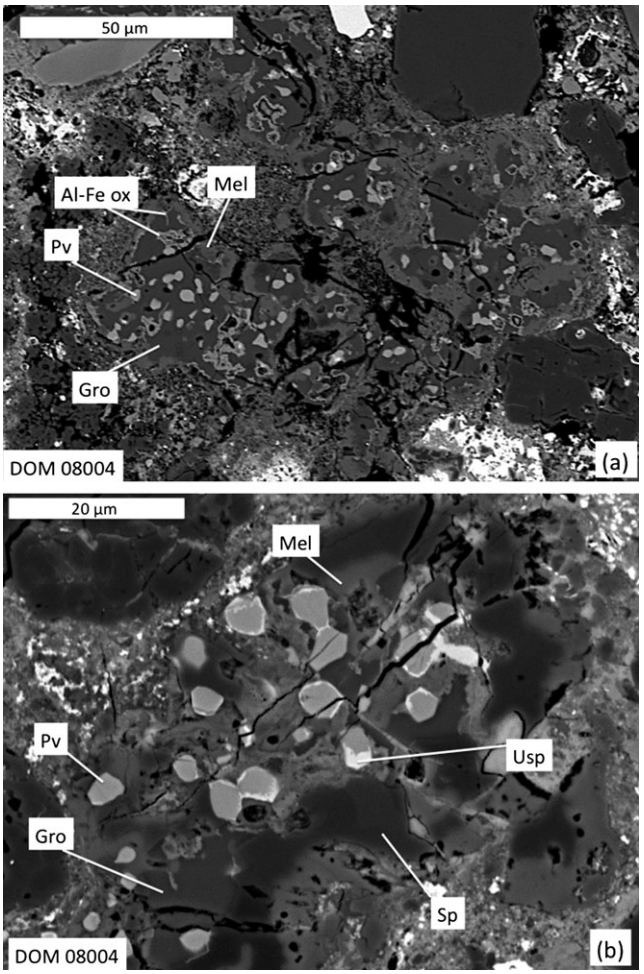

Fig. 5. Backscattered electron images of grossite-bearing, hibonite-free inclusions. Abbreviations as in Fig. 2, plus Gro = grossite; Al-Fe ox = Al-, Fe-bearing oxide. a) DOM 08004 grossite-perovskite-melilite inclusion 75-1. b) DOM 08004 grossite-melilite-spinel-perovskite inclusion 29-6. Perovskite is partially altered to ulvöspinel, Fe_2TiO_4 (Usp).

thin veins of FeO-rich oxide, but the spinel in which it is enclosed does not. The inclusion is enclosed in anorthite of the host object. Inclusion 26-1 (Fig. 6e) consists of the coarsest hibonite found in DOM 08004. The grain is 50 × 30 μm, appears to be a fragment of a once-larger object, with grossite and alteration products adjacent to it, and fine (1–2 μm) inclusions of a Sc-, Zr-, Y-oxide. In transmitted light, the hibonite in 26-1 is strongly pleochroic from colorless to blue. In 88-1 (Fig. 6f), hibonite and spinel are the dominant phases, intergrown in a texture typical of many spinel-hibonite spherules found in CM2 chondrites (e.g., MacPherson et al. 1983; Ireland 1990). Minor amounts of grossite and melilite are present, along with trace amounts of perovskite and Al-, Fe-oxide.

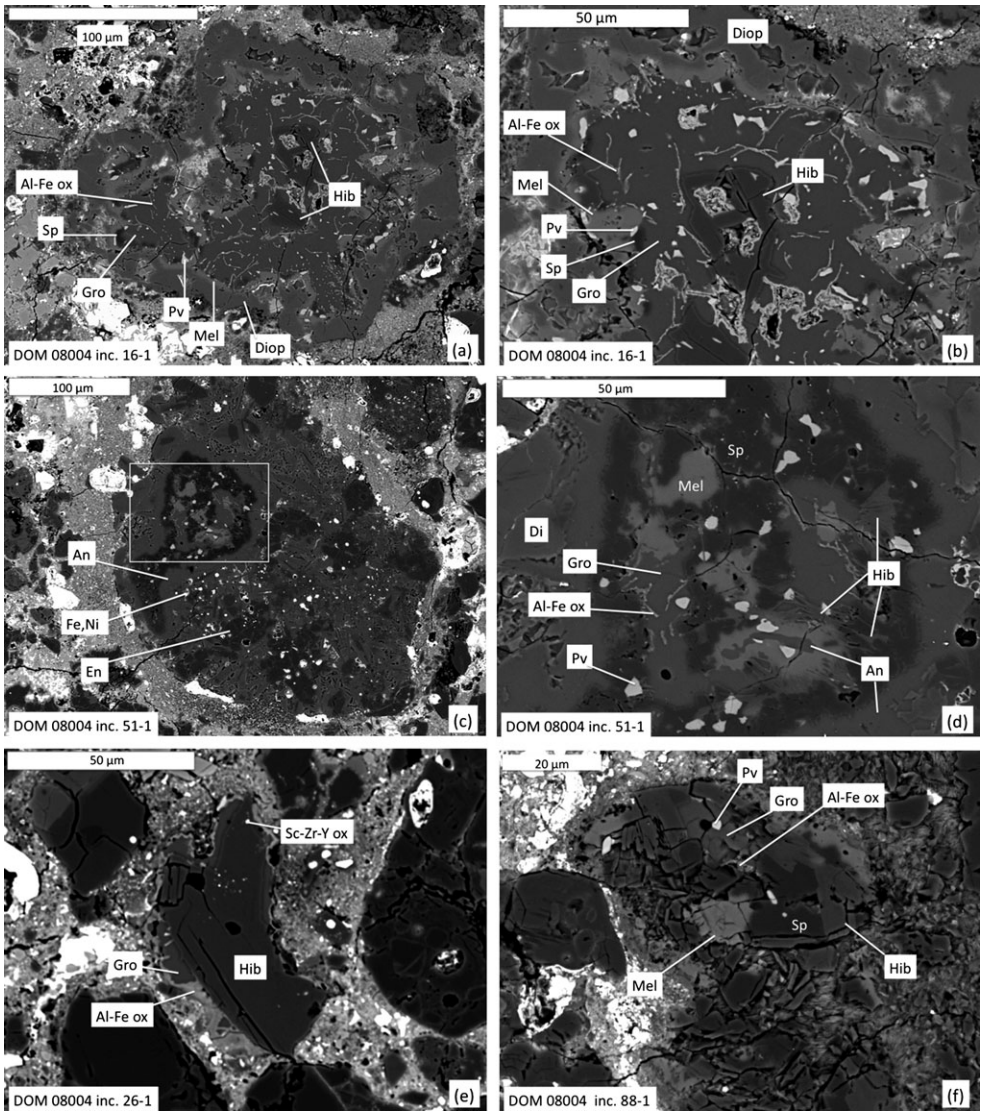

Fig. 6. Backscattered electron images of hibonite-, grossite-bearing inclusions in DOM 08004. Abbreviations as used previously. a) Inclusion 16-1. View of entire inclusion, showing thin melilite and thick diopside rim layers enclosing the grossite-dominated inclusion. b) Higher-magnification view of inclusion 16-1. c) Grossite-, hibonite-bearing inclusion 51-1 (in box), which is enclosed in a fragment of an aluminum-rich chondrule. An = anorthite. En = enstatite. d) Area outlined in (c), the hibonite-, grossite-bearing inclusion. e) Hibonite-rich inclusion fragment 26-1. There is grossite adjacent to hibonite, which has fine inclusions of Sc-, Zr-, Y-oxide. f) Hibonite-, spinel-rich inclusion 88-1, with minor grossite and melilite.

One hibonite-, grossite-bearing inclusion was found in DOM 08006. It is ~75 µm across with intergrown spinel and hibonite that enclose grossite pockets. The spinel/hibonite intergrowth is enclosed in melilite and the object has a pyroxene rim.

Sc-Rich Inclusion

By far the most refractory inclusion found is 22-4 (Fig. 7), a Sc-rich spherule fragment ~50 µm across consisting of anhedral, Y-, Zr-, REE-rich perovskite enclosed in a Sc-, Al oxide. The latter, represented by the bright areas in the Sc X-ray map (Fig. 7b), is an occurrence of a recently reported phase with the endmember formula $Ca_2Sc_6Al_6O_{20}$ (Ma et al. 2014), found in Murchison and Vigarano. It also contains Mg, Ti, V, Fe, Zr, and REE at levels that are detectable by electron microprobe. The inclusion is partially enclosed in rims of melilite and davisite (Sc-rich pyroxene). This inclusion may be "ultrarefractory," but to truly define it as such would require measurement of its complete chondrite-normalized rare Earth element pattern and

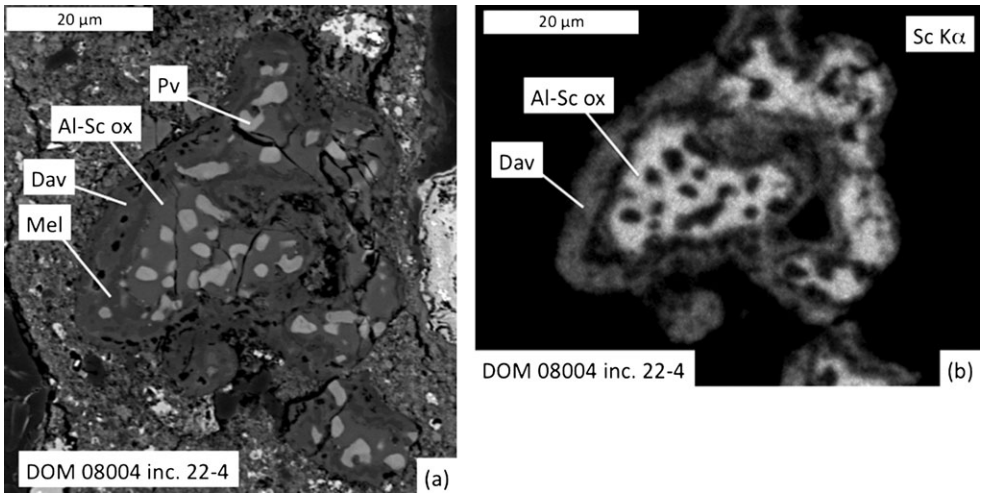

Fig. 7. Sc-rich inclusion 22-4 in DOM 08004. a) Backscattered electron image. Al-Sc ox = Al-, Sc-oxide; Dav = davisite. b) Sc Kα X-ray map. The brightest areas are the most Sc-rich.

identification of it as complementary to a Group II pattern (Mason and Martin 1977), and these data are not available.

Rims on Inclusions

Rims are found on 50–60% of the inclusions in the DOM samples and Acfer 094, and the rims are mineralogically similar; in these three samples, 26–33% of the inclusion populations have pyroxene (typically aluminous diopside) rims (e.g., Figs. 2a and 2b), 10–15% have melilite rims (e.g., Fig. 5a), and 5–10% have a layer of each phase (e.g., Figs. 4a and 6). In both DOM 08004 and Acfer 094, almost every spinel-perovskite inclusion has a melilite rim, and almost every spinel-melilite inclusion has a pyroxene rim. In contrast, in ALHA77307, only 33% of the inclusions have rims, pyroxene rims are much more common than melilite rims (85% of rims are pyroxene, 9% are melilite) and the occurrence of rims is evenly distributed among the inclusion types. In this sample, 28% of the inclusions have pyroxene rims, only 3% have melilite, and none have layers of both.

Mineral Chemistry

As is typical of CO3.0 chondrites and Acfer 094, high proportions of the CAIs in DOM 08004 and DOM 08006 contain melilite. Compositions in the present samples are gehlenitic, with average åkermanite contents of 7.8 mole% in DOM 08004 and 8.5 mole% in DOM 08006. Representative analyses are given in Table 2 and histograms of åkermanite contents are shown in Fig. 8. Except for one analysis, the range of compositions in both samples is $Åk_{0–20}$. The typical composition range within an inclusion is ~5 mole% Åk. The DOM 08004 data set includes six analyses of melilite rims. Their range, $Åk_{2–12}$, is similar to that of the most common compositions in the populations in both DOM 08004 and 08006. All analyses have very low Na_2O contents, ≤0.06 wt%.

Hibonite-bearing inclusions also are a major component of the CAI populations in the DOM and ALHA samples. Representative electron probe analyses of hibonite are given in Table 3. Endmember hibonite is $CaAl_{12}O_{19}$ and a common substitution is Mg^{2+} + (Ti^{4+}, Si^{4+}) for two Al^{3+} cations, so that Mg contents are typically strongly correlated with Ti+Si cation abundances, as in Fig. 9a. If Fe present in hibonite substituted for Mg, as it commonly does in Mg-bearing phases, then the fit to a 1:1 line can be improved by plotting Mg+Fe against Ti+Si, but for the present samples, as was seen with Acfer 094 (Simon and Grossman 2011), the data fall above the 1:1 line on such a plot (Fig. 9b). A plot of Fe versus Mg cations per 19 oxygen (Fig. 9c) shows that they are not correlated, indicating that Fe did not preferentially substitute for Mg, explaining why the Mg+Fe cation totals tend to be greater than the corresponding Ti+Si abundances. Hibonite compositions in DOM 08004 and ALHA77307 reach higher Ti contents than the hibonite found in DOM 08006. The Ti contents of hibonite do not correlate with the presence or absence of coexisting grossite.

Spinel compositions in DOM 08004 and 08006 inclusions are near-endmember $MgAl_2O_4$ with a few exceptions. Almost all TiO_2, V_2O_3, and Cr_2O_3 contents are <0.5 wt%. One inclusion, with hibonite and spinel poikilitically enclosed in gehlenitic melilite, has spinel with ~0.6 wt% V_2O_3. Most FeO contents are between

Table 2. Representative electron microprobe analyses of melilite in DOM 08004 and DOM 08006.

	1	2	3	4	5	6	7	8
Na_2O	BDL	0.03	BDL	BDL	0.03	BDL	0.02	0.02
MgO	0.69	1.87	0.49	1.42	1.54	1.54	0.86	1.58
Al_2O_3	35.05	31.79	35.61	33.36	32.34	32.97	34.96	32.66
SiO_2	22.84	24.56	21.97	23.66	24.33	23.33	22.46	23.76
CaO	41.30	41.62	40.51	41.44	40.44	40.83	40.71	40.44
TiO_2	0.06	BDL	0.11	0.10	0.05	BDL	0.07	BDL
FeO	0.45	0.33	0.17	0.61	0.85	0.33	0.61	0.88
SUM	100.42	100.25	98.88	100.63	99.57	99.00	99.72	99.41
Cations per 7 oxygen anions								
Na	0	0.002	0	0.001	0.002	0.000	0.002	0.002
Mg	0.047	0.127	0.034	0.097	0.106	0.107	0.059	0.109
Al	1.885	1.714	1.941	1.793	1.752	1.798	1.894	1.776
Si	1.042	1.123	1.016	1.079	1.119	1.080	1.033	1.096
Ca	2.019	2.040	2.008	2.025	1.992	2.024	2.005	1.999
Ti	0.002	0.000	0.004	0.003	0.002	0.000	0.002	0.000
Fe	0.017	0.013	0.007	0.023	0.033	0.013	0.023	0.034
Total	5.013	5.019	5.010	5.022	5.005	5.021	5.019	5.015
Åk (mole%)	4.9	13.1	2.6	9.3	11.6	9.6	4.8	10.6

Analyses 1–5: DOM 08004. 6–8: DOM 08006. 1, 2: Inclusion 26-2 (Fig. 2a). 3: 51-1 (Fig. 6d). 4: 32-1 (Fig. 3d). 5: 75-1. Rim of a grossite-perovskite-melilite inclusion. 6: 1–2 (Fig. 2b). 7: 11-7, melilite-spinel-perovskite inclusion. 8: 11-6, melilite-spinel-perovskite inclusion. BDL = below detection limit of electron probe of 0.024 wt% Na_2O or 0.042 wt% TiO_2.

0.2 and 1.1 wt%, with the exception of one inclusion in DOM 08004, 29-5 (Fig. 10), which has grains with FeO contents from 3.2 to 8.8 wt%. The grains are not monotonically zoned, with sharp contacts and two triple junctions (Fig. 10a). An electron probe traverse across one of the contacts shows FeO contents ranging from 3.6 to 8.8 wt% over just 4 μm (Fig. 10b).

Grossite compositions in both meteorites are also nearly pure except for 0.2–1.0 wt% FeO, with very low MgO and TiO_2 contents, as shown by the representative analyses given in Table 4.

There are mainly two types of pyroxene in DOM 08004 and 08006 inclusions: Al-diopside occurring as rims on inclusions, and fine-grained, Ti-rich pyroxene occurring intergrown with spinel in CAI interiors or as a thin rim layer. The latter has TiO_2^{tot} contents of 6.3–15 wt%, V_2O_3 from 0.26 to 0.78 wt%, and Sc_2O_3 contents ranging from below detection to 0.14 wt% (Table 5). An unusual pyroxene in the Sc-rich inclusion in DOM 08004, 22-4 (Fig. 7), has ~16–18 wt% Sc_2O_3 and is not very Ti-rich (between 1 and 2 wt% Ti as TiO_2). This pyroxene, in which Sc is the dominant cation in the M1 site, is davisite (Ma and Rossman 2009). As shown in Table 5, the pyroxene in 22-4 is Sc-rich and Ti-poor compared to the davisite type material (Ma and Rossman 2009), indicating that it has a higher proportion of the ideal davisite endmember ($CaScAlSiO_6$).

Compositions of the Sc aluminate found in 22-4 are given in Table 6 along with analyses of occurrences of the phase found in inclusions in the Murchison (CM2) and Vigarano (CV3) chondrites by Ma et al. (2014). The abundances of the major and minor elements in the DOM occurrence are quite similar to those reported by Ma et al. (2014), although the present samples have slightly lower Ti^{3+}/Ti^{tot} ratios than the Murchison occurrence, and in the Vigarano occurrence all of the Ti is trivalent. Ma et al. (2014) reported that the Murchison material is very ^{16}O-rich ($\Delta^{17}O \sim -24 \pm 3‰$).

DISCUSSION

Identification of Pristine Chondrites

Many meteorites contain materials that have nebular origins, but few meteorites that contain such materials have undergone little or no metamorphism on the parent bodies of their hosts. One way to assess the pristinity of chondrites is through fine-scale study of their matrix mineralogy, and another is by measurement of Cr_2O_3 contents and variability in olivine.

With increasing metamorphic grade, matrix assemblages become increasingly equilibrated with respect to Fe/Mg ratios of ferromagnesian silicates, amorphous silicates become crystalline, and presolar grains are destroyed. During aqueous alteration, presolar silicates and oxides, unlike SiC, are destroyed (Davidson et al. 2008, 2009; Floss and Stadermann 2012). Thus, chondrites that have unequilibrated matrices with amorphous silicates and high contents of presolar oxygen-rich grains are considered pristine;

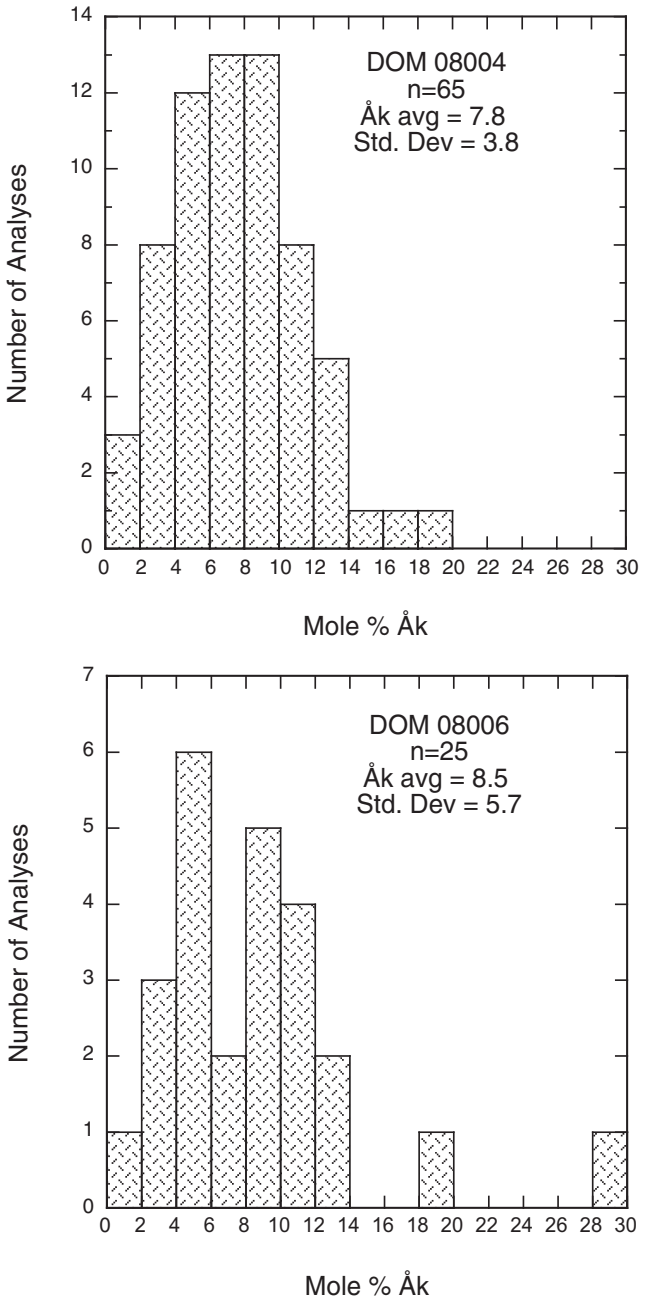

Fig. 8. Histograms of melilite compositions (åkermanite contents) in DOM 08004 and in DOM 08006, determined by electron microprobe.

DOM 08006, ALHA77307, and Acfer 094 are examples of such chondrites (Brearley 1993; Greshake 1997; Brunner and Brearley 2011; Stroud et al. 2013). These samples have some of the highest matrix-normalized contents of presolar O-rich grains that have been observed (Vollmer et al. 2009; Nguyen et al. 2010; Floss and Stadermann 2012; Nittler et al. 2013).

In a study of the first stages of the effects of metamorphism of chondrites, Grossman and Brearley (2005) found that with increasing grade among ordinary and CO3 chondrites, the mean Cr_2O_3 content of ferroan olivine decreases slightly and its standard deviation (σ) increases from grade 3.0 through 3.1 as Cr is mobilized. With further increase in grade through 3.2, both the Cr_2O_3 contents and σ decrease. The trend for unequilibrated ordinary chondrites differs from that of the CO3s in that it starts at higher mean Cr_2O_3 contents and the σ values increase more sharply and reach higher values before decreasing.

In this study, data were collected for both DOM samples, and they are plotted in Fig. 11 along with literature data for CO3s and Acfer 094 for comparison. Our result for DOM 08006 is very close to that for Acfer 094 (Grossman and Brearley 2005), with a slightly higher σ and slightly lower average Cr_2O_3 content than the values reported for DOM 08006 by Davidson et al. (2014). All three points, along with reported data for ALHA77307 (Grossman and Brearley 2005), are within the range of values for CO3.0 chondrites and well off the ordinary chondrite trend. Our analyses of olivine in DOM 08004 yield a lower mean Cr_2O_3 content than that of DOM 08006, and they indicate a grade of 3.1 (Fig. 11). The Cr data indicate that all four of these samples experienced very limited degrees of metamorphism, in agreement with inferences from the presolar grain and amorphous silicate contents of their matrices. The absence of diffusion gradients between

Table 3. Representative electron probe analyses of hibonite in DOM 08004 and DOM 08006.

	1	2	3	4	5
MgO	4.29	0.93	0.71	1.52	0.95
Al_2O_3	80.16	87.24	88.34	87.93	88.18
SiO_2	0.29	0.05	0.03	0.17	0.36
CaO	8.25	8.72	8.57	8.51	8.79
Sc_2O_3	0.03	0.04	0.53	BDL	BDL
TiO_2	7.18	1.97	1.56	2.05	2.24
V_2O_3	0.12	BDL	0.03	BDL	BDL
FeO	0.27	0.25	0.46	0.57	0.74
SUM	100.58	99.21	100.22	100.76	101.28
Cations per 19 oxygen anions					
Mg	0.720	0.156	0.119	0.251	0.158
Al	10.644	11.610	11.665	11.532	11.517
Si	0.032	0.005	0.003	0.019	0.040
Ca	0.996	1.055	1.029	1.014	1.043
Sc	0.001	0.002	0.026	0	0
Ti	0.609	0.167	0.132	0.171	0.186
V	0.006	0	0.001	0	0
Fe	0.026	0.024	0.043	0.053	0.069
Total	13.034	13.018	13.017	13.040	13.013

Analysis 1: DOM 08004, inclusion 12-1. 2: DOM 08004, inclusion 16-1. 3: DOM 08004, inclusion 26-1. 4: DOM 08006, inclusion 1-1. 5: DOM 08006, inclusion 10-2. BDL = below the detection limit of 0.03 wt% Sc_2O_3 or V_2O_3.

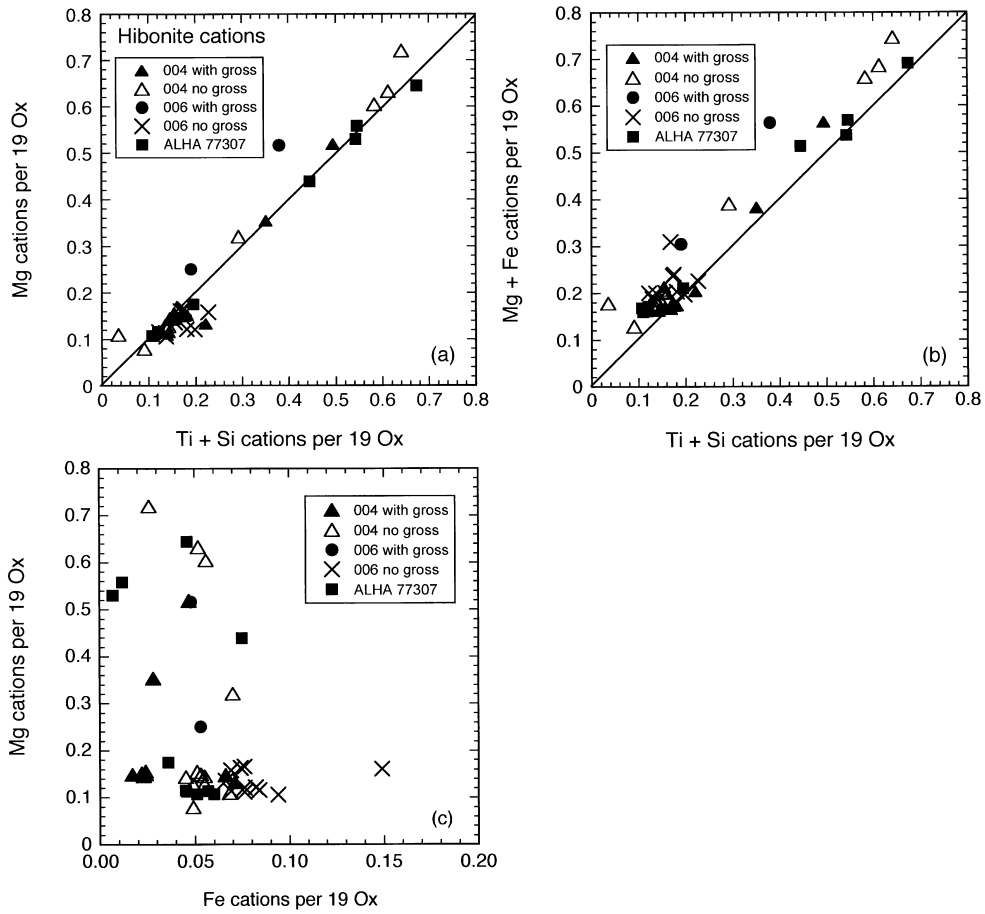

Fig. 9. Hibonite compositions, in terms of cations per 19 oxygen anions, in DOM 08004 (004), DOM 08006 (006), and ALHA77307. Data for inclusions with and without grossite are identified. a) Mg versus Ti+Si cations. b) Mg+Fe versus Ti+Si cations. c) Mg versus Fe cations.

spinel grains of contrasting composition in the inclusion shown in Fig. 10 also shows that any post-accretion heating was very limited.

Comparison of CAIs in DOM with Those in ALHA77307 and Acfer 094

Grossite-bearing inclusions are very rare in CO3 chondrites and are somewhat less rare in DOM 08004 and DOM 08006. Based on the abundances of grossite-bearing inclusions found in them, the DOM samples are not typical CO3 chondrites. Another comparable type of meteorite, also with high presolar grain contents and similar proportions of grossite-bearing inclusions, is the ungrouped carbonaceous chondrite Acfer 094. The FeO contents of nominally FeO-free phases in refractory inclusions provide a useful basis for comparison of the present samples with Acfer 094 and CO3 chondrites. A study by Simon and Grossman (2011) found that most phases in most of the Acfer 094 refractory inclusions that they analyzed contained distinctive, remarkably high FeO contents, between 0.5 and 1.5 wt%. The FeO contents of hibonite, grossite, melilite, and spinel in DOM 08004 and 08006 are compared with those of their counterparts in Acfer 094 in Fig. 12. Analyses of inclusions in ALHA77307 were collected for this study and are plotted for comparison as well, to see if the DOM compositions are like those of phases in inclusions in a typical CO3, or if they are more like Acfer 094.

Hibonite analyses are plotted in Fig. 12a. Typical FeO contents of hibonite in DOM 08006 are 0.5–1.0 wt%. Most FeO contents of DOM 08004 hibonite are between 0.3 and 0.8 wt%. One inclusion yielded two analyses with <0.3 wt% FeO. In Acfer 094, most hibonite has between 0.5 and 1.2 wt%. Exceptions include hibonite with 1.2–2.7 wt% in inclusion L5-1 (Simon and Grossman 2011) and an inclusion (ACM4) with FeO-poor hibonite (0.1–0.2 wt%). Hibonite in ALHA77307 has 0.1–0.8 wt% FeO, with most analyses

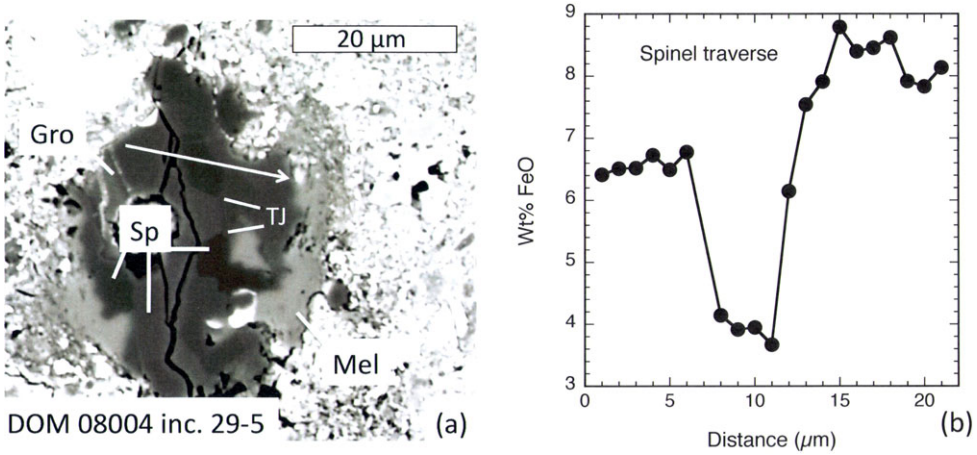

Fig. 10. Unusual spinel-rich inclusion 29-5 in DOM 08004. a) Backscattered electron image. The contrasting albedos of the spinel grains reflect differing FeO contents. Arrow indicates the location of an electron probe traverse, the results of which are shown in (b), a plot of FeO contents in spinel versus distance. TJ = triple junction.

Table 4. Representative electron probe analyses of grossite in DOM 08004 and DOM 08006.

	1	2	3	4	5	6	7
MgO	0.04	0.11	0.05	0.03	0.04	0.05	0.06
Al_2O_3	77.49	77.97	77.33	77.79	76.35	77.18	77.19
SiO_2	0.07	0.06	0.34	0.03	0.07	0.08	0.06
CaO	22.11	21.81	21.38	22.26	21.91	21.83	21.72
TiO_2	0.13	0.06	0.08	0.18	0.15	0.09	0.08
FeO	0.28	0.18	0.73	0.73	0.70	0.43	0.88
SUM	100.12	100.18	99.92	101.03	99.21	99.66	99.99
Cations per 7 oxygen anions							
Mg	0.002	0.007	0.003	0.002	0.003	0.003	0.004
Al	3.963	3.977	3.959	3.952	3.950	3.966	3.960
Si	0.003	0.002	0.015	0.001	0.003	0.003	0.002
Ca	1.028	1.011	0.995	1.028	1.030	1.020	1.013
Ti	0.004	0.002	0.003	0.006	0.005	0.003	0.003
Fe	0.010	0.006	0.027	0.026	0.026	0.016	0.032
Total	5.011	5.007	5.001	5.016	5.017	5.011	5.014

1: DOM 08004, inclusion 16-1. 2: DOM 08004, inclusion 51-1. 3: DOM 08004, inclusion 75-1. 4: DOM 08004, inclusion 29-6. 5: DOM 08004, inclusion 77-1. 6: DOM 08006, inclusion 1-1. 7: DOM 08006, inclusion 9-3.

≤0.6 wt%. Han (2014) found a range of 0.4–0.8 wt% FeO in the 10 ALHA77307 hibonite analyses they obtained from two inclusions.

Grossite analyses are compared in Fig. 12b. Whereas grossite-bearing inclusions were easily found in the DOM and Acfer samples, none were found in ALHA77307. Elevated FeO and MgO contents are seen in most DOM and Acfer analyses compared to grossite in CAIs in CH chondrites (Kimura et al. 1993; Weber and Bischoff 1994). The 20 analyses reported in the latter work average 0.3 wt% FeO, while contents >0.4 wt% are common in DOM and Acfer. The grossite analyses, with <0.4 wt% FeO shown in Fig. 12b, are from two inclusions in DOM 08004: 16-1, the large, grossite-rich inclusion (Figs. 6a and 6b); and 51-1 (Figs. 6c and 6d), the grossite-bearing inclusion that is enclosed in an Al-rich chondrule fragment. The grossite in both of these inclusions is relatively FeO-poor despite hosting veins of an Fe-bearing oxide, a secondary alteration product seen in many of the grossite-bearing inclusions in DOM 08004. The veins are Na-bearing and a terrestrial origin cannot be ruled out, but the primary phases, including melilite, in the inclusions are very Na-poor. In an inclusion with just a trace of this material, 88-1 (Fig. 6f), the grossite has 0.5 wt% FeO, a higher content than seen in the vein-rich inclusion 16-1, and the hibonite and melilite in this inclusion have FeO contents that are typical for these phases in DOM 08004: 0.24–0.70 wt% FeO in hibonite and 0.34–0.38 wt% in melilite. The presence of veins

Table 5. Compositions of Ti- or Sc-rich pyroxene in inclusions in DOM 08004.

	1[a]	2[a]	3[a]	4	5	Davisite[b]
MgO	7.68	8.00	6.50	5.61	4.54	2.82
Al_2O_3	23.58	21.28	23.12	15.87	16.68	21.05
SiO_2	32.96	33.02	32.89	32.15	31.05	26.24
CaO	24.93	24.66	24.85	26.09	25.23	23.55
Sc_2O_3	0.03	0.11	0.12	16.53	18.04	14.70
TiO_2	10.01	12.69	11.44	1.32	1.51	8.66
V_2O_3	0.69	0.27	0.78	0.72	0.79	0.55
Cr_2O_3	0.06	0.05	0.03	0.04	0.03	NR
FeO	0.37	1.00	0.58	0.98	0.97	0.30
SUM	100.30	101.07	100.30	99.31	98.86	97.87
Ti_2O_3	2.23	3.45	5.73	ND	ND	4.64
TiO_2	7.50	8.74	5.10	ND	ND	3.57
Sum	100.03	100.58	99.69	99.31	98.86	97.42
Ti_2O_3+TiO_2	9.73	12.19	10.83	ND	ND	8.21
Cations per 6 oxygen anions						
Si	1.226	1.227	1.239	1.252	1.217	1.028
Al	0.774	0.773	0.761	0.729	0.771	0.972
Al	0.260	0.159	0.266	0	0	0
Mg	0.426	0.443	0.365	0.326	0.265	0.165
Fe	0.012	0.031	0.018	0.032	0.032	0.010
Sc	0.001	0.004	0.004	0.561	0.616	0.502
V	0.019	0.007	0.022	0.022	0.025	0.017
Cr	0.002	0.002	0.001	0.001	0.001	–
Ti^{3+}	0.070	0.108	0.180	–	–	0.152
Ti^{4+}	0.211	0.247	0.144	0.039	0.045	0.105
Ca	1.000	1.000	1.000	1.089	1.060	0.989
Total	4.000	4.000	4.000	4.052	4.032	3.940

1: Ti-rich pyroxene in DOM 08004, 22-1, a spinel-pyroxene-anorthite spherule. 2: Ti-rich pyroxene in DOM 08004, 35-1, a spinel-pyroxene-perovskite spherule fragment. 3: Ti-rich pyroxene in DOM 08004, 37-2, a spinel-pyroxene inclusion. 4 and 5: Davisite in DOM 08004, 22-4. NR: not reported. ND: not determined.

[a]Analyses normalized to one Ca and four total cations per six oxygen anions.

[b]Analysis of davisite from Allende (Ma and Rossman 2009); also contains the following (in wt%): ZrO_2: 2.00; Y_2O_3: 0.56; Dy_2O_3: 0.27; Gd_2O_3: 0.13; and Er_2O_3: 0.08.

does not appear to be related to FeO-enrichment of grossite.

Melilite analyses are illustrated in Fig. 12c. Again, a high degree of overlap between the suites of DOM and Acfer analyses is seen, with FeO contents mostly 0.2–1.2 wt%. The eight analyses of melilite in Acfer 094 CAIs in table AE2 of Krot et al. (2004) average ~0.3 wt% FeO, but, like Simon and Grossman (2011), they found FeO in every CAI phase they analyzed (Krot, personal communication). It is worth noting that very low Na_2O contents are reported for Acfer 094 melilite: <0.021 wt % by Simon and Grossman (2011); and <0.06 wt% by Krot et al. (2004), so its FeO enrichments are not due to Na-Fe metasomatism, and melilite in both DOM samples also has very low Na_2O contents (Table 2). There is less overlap between the DOM samples and ALHA77307 than with Acfer, as lower FeO contents, mostly <0.3 wt%, are found in melilite in ALHA77307, both in the present analyses and those of Han (2014).

A plot of FeO versus Cr_2O_3 in spinel also shows extensive overlap among the sample suites (Fig. 12d). Even with the anomalous, FeO-rich DOM 08004 inclusion 29-5 not plotted, spinel in 08004 inclusions reaches higher FeO contents than inclusions in the other samples considered here. Some spinel with relatively Cr-rich compositions is found in Acfer 094.

Overall, among the data plotted in Fig. 12, there is extensive overlap between the DOM 08004 and 08006 analyses, and the DOM samples exhibit stronger overlap with Acfer 094 data than with ALHA77307 analyses.

The FeO enrichments of refractory phases in DOM 08004 were obtained independent of, and Na_2O contents were unaffected by, the formation of alteration products, and there is no evidence for reaction with the matrix. It is therefore quite likely that the FeO enrichments of hibonite, grossite and melilite in DOM inclusions reflect an early exposure to an FeO-rich

Table 6. Representative electron probe analyses of the Sc-rich oxide in DOM 08004 inclusion 22-4, and in Murchison and Vigarano.

	1	2	3	MURCH	VIG
MgO	1.43	1.61	1.51	1.21	1.49
Al_2O_3	38.95	37.24	37.04	39.52	36.80
SiO_2	0.16	0.29	0.34	NR	2.09
CaO	15.28	15.31	15.15	14.83	15.05
Cr_2O_3	0.06	0.08	0.07	NR	NR
Sc_2O_3	32.58	34.95	34.66	33.76	34.03
TiO_2^{tot}	7.40	6.96	7.20	6.91	4.79
TiO_2	4.25	3.99	4.01	2.58	0.00
Ti_2O_3	2.83	2.67	2.91	3.90	4.31
V_2O_3	0.32	0.82	0.70	NR	1.59
FeO	0.96	0.89	1.10	0.46	1.47
Y_2O_3	0.93	0.70	0.81	0.84	0.27
ZrO_2	2.97	3.42	3.19	3.33	3.40
Gd_2O_3	BDL	BDL	BDL	0.30	NR
Dy_2O_3	0.24	0.16	0.20	0.47	NR
SUM	101.00	102.16	101.70	101.20	100.50
Cations per 20 oxygen anions					
Mg	0.293	0.329	0.309	0.25	0.31
Al	6.322	6.011	6.008	6.42	5.98
Si	0.022	0.039	0.047	0.00	0.29
Ca	2.254	2.245	2.233	2.19	2.22
Cr	0.007	0.009	0.008	0	0
Sc	3.909	4.169	4.155	4.05	4.09
Ti^{4+}	0.440	0.411	0.415	0.27	0.00
Ti^{3+}	0.326	0.305	0.335	0.45	0.50
V	0.035	0.090	0.078	0	0.18
Fe	0.111	0.102	0.127	0.05	0.17
Y	0.069	0.051	0.060	0.06	0.02
Zr	0.199	0.228	0.214	0.22	0.23
Gd	0	0	0	0.01	0
Dy	0.011	0.007	0.009	0.02	0
Total	13.997	13.997	13.997	13.99	13.99
Ti^{3+}/Ti^{tot}	0.425	0.426	0.446	0.625	1.000

Analyses 1–3: DOM 08004, inclusion 22-4. MURCH, VIG: Occurrences in Murchison and Vigarano, respectively, from Ma et al. (2014). Ti^{3+}/Ti^{4+} ratios calculated to yield 14 total cations per 20 oxygen anions. BDL = below the detection limit of electron probe of 0.052 wt% Gd_2O_3. NR = not reported by Ma et al. (2014).

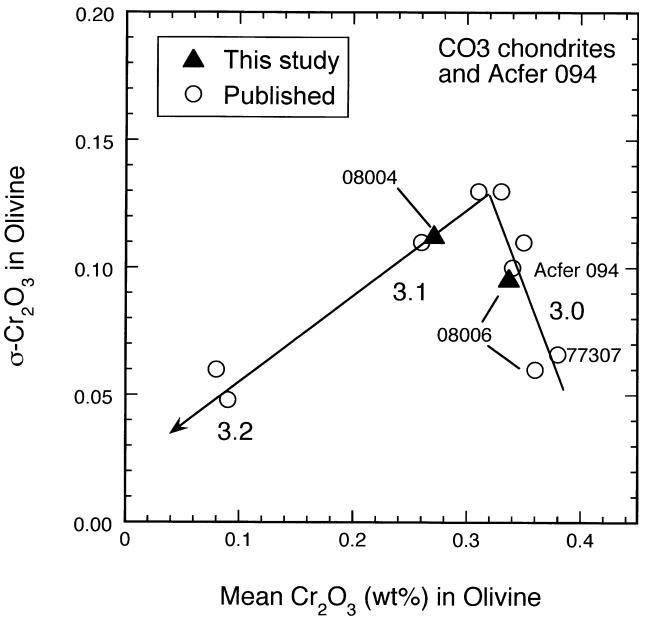

Fig. 11. Plot of standard deviation (σ) versus mean Cr_2O_3 content for suites of analyses of ferroan (>2 wt% FeO) olivine in CO3 chondrites and the ungrouped C3 Acfer 094. With increasing metamorphic grade from 3.0 to 3.1, average Cr_2O_3 contents decrease and σ increases, and with further increase in grade, σ decreases. Published analysis of DOM 08006 is from Davidson et al. (2014); it plots at the low-grade end of the trend. Other published data are from Grossman and Brearley (2005).

environment, as inferred for inclusions in Acfer 094 (Simon and Grossman 2011). It is interesting to note that a recent study has yielded additional evidence for such a stage in the formation of Acfer 094. Cuvillier et al. (2014a) found that some forsterite grains in its matrix have thin, fayalitic ($Fa_{40–50}$) rims and that some Fe/Mg diffusion occurred between the rims and the host grains, but not between the rims and adjacent, relatively FeO-rich amorphous silicates. Because not all forsterite grains have fayalitic rims and there was no equilibration of rims and other matrix phases, Cuvillier et al. (2014a) concluded that rim formation occurred in a pre-accretionary, FeO-rich environment. These observations contrast with the results of an analogous investigation of Allende by the same group (Cuvillier et al. 2014b), in which fayalitic overgrowths found on isolated forsterite grains were described and analyzed. In Allende, the overgrowths on forsterite are similar in composition and microstructure to the fine, fayalitic (Fa_{50}) matrix grains, leading those workers to conclude that the matrix and overgrowths had a common origin and thermal history. The presence of FeO-rich phases (oxide stringers, ulvöspinel) in DOM inclusions and their absence from Acfer 094 inclusions may be an indication that the oxidizing environment to which the former were exposed was more FeO-rich and/or longer-lived than that to which the Acfer inclusions were exposed.

Formation of Unusual Inclusions

One of the largest inclusions found in DOM 08004, 16-1 (Figs. 6a and 6b), is also one of the more unusual ones. One inclusion that can be considered analogous to it has been reported: inclusion 022/19, from the CH chondrite Acfer 182 (Weber and Bischoff 1994). That inclusion also has a porous, hibonite-rich core enclosed in a mantle of grossite with fine grains of perovskite throughout. The rims of the inclusions have similar

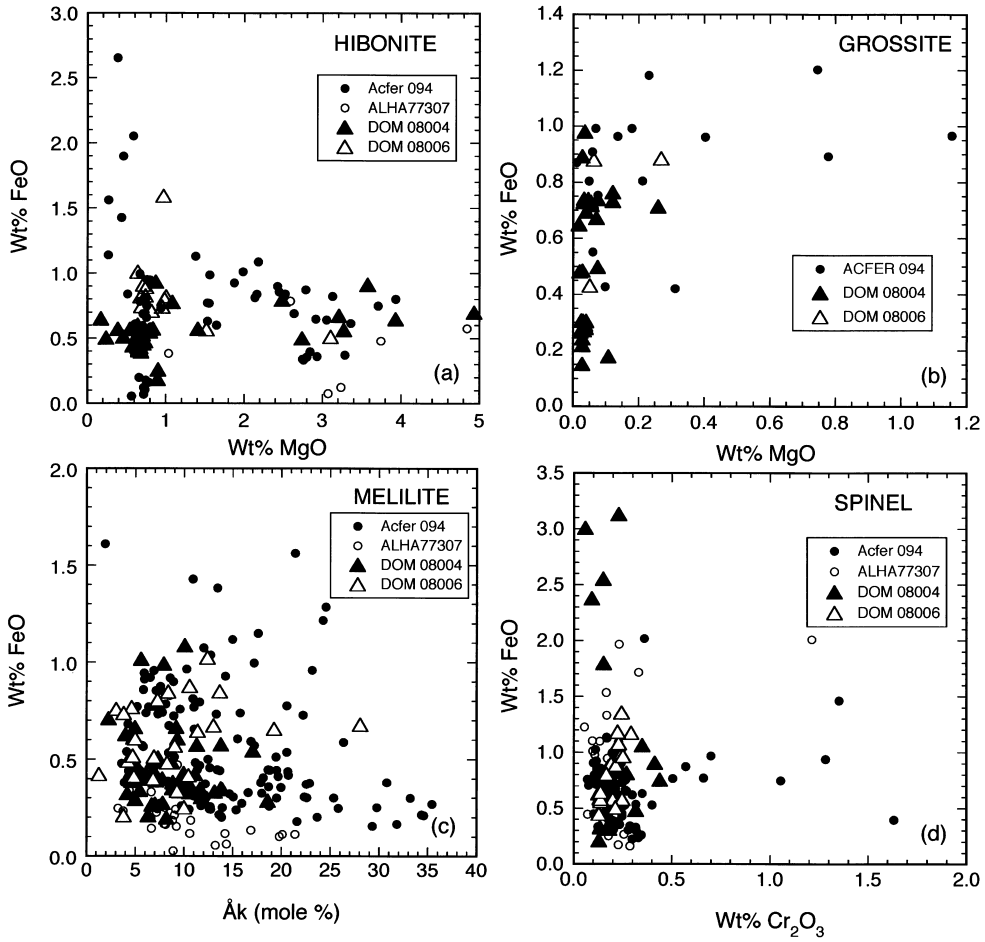

Fig. 12. Comparison of FeO contents of nominally FeO-free phases in refractory inclusions in DOM 08004, DOM 08006, Acfer 094, and ALHA77307. Much overlap is seen between the DOM and Acfer samples, somewhat less between DOM and ALHA. a) Hibonite. b) Grossite (none found in ALHA77307). c) Melilite. d) Spinel.

mineralogical compositions but different textures and different proportions of phases. Whereas 16-1 has a thin, ragged layer of melilite, with spinel occurring sparsely along the grossite/melilite contact, and a thick outer layer of clinopyroxene, the rim layers in the Acfer inclusion are more well-defined, with a spinel+hibonite layer mantled by a uniform, ribbon-like melilite layer and a very thin, outermost layer of Ca-rich pyroxene. Both inclusions, with phases becoming less refractory from their cores outward, probably formed by condensation of hibonite and grossite followed by rim formation. Weber and Bischoff (1994) did not speculate on the conditions of rim formation but noted that hibonite in the rim differed from that in the core morphologically and chemically, and they concluded that the two generations of hibonite formed in different events under different conditions. Calculations by Grossman (2010) show that, after early condensation of hibonite and grossite, during continued equilibrium condensation with decreasing temperature, melilite growth would consume enough Ca relative to Al from the residual oxides to re-stabilize hibonite, and this hibonite would eventually react completely with gaseous Mg to form spinel; with continued decreasing temperature, melilite would react with the residual gas to form clinopyroxene. The textures of 16-1 and 022/19 are remarkably consistent with this sequence. In the latter inclusion, the late hibonite was not completely consumed to form spinel. In 16-1, either it did react completely or is present but not exposed in the plane of the section.

Inclusion 51-1 (Figs. 6c and 6d) is possibly the first relict, grossite-bearing refractory inclusion found that is not in a CH chondrite. In general, grossite-bearing inclusions are rare, as are relict CAIs. It is not surprising that the host chondrule is Al_2O_3-rich, however; according to Krot et al. (2006), >15% of Al-rich chondrules contain relict CAIs, a much higher proportion than they found for ferromagnesian chondrules (just 5 in >10,000). The compact texture of

the refractory inclusion and the many rounded grain boundaries suggest that it crystallized from a liquid. The texture of hibonite laths penetrating perovskite grains was also observed in a grossite-bearing inclusion in Acfer 094 that was interpreted by Simon and Grossman (2011) to have an igneous origin.

The very Sc-rich inclusion, 22-4 (Fig. 7), is a fragment of a spherule that formed by melting of a Sc-rich, highly refractory oxide assemblage, probably early condensate grains. After it reached temperatures at which silicates were stable, the spherule reacted with the nebular gas to form the outer layers of melilite and davisite, providing the Sc that stabilized the latter.

Classification of DOM 08004 and DOM 08006

As Fig. 11 shows, analyses of Cr oxide contents in ferroan olivine in both DOM 08004 and 08006 plot along the CO trend, and the values are consistent with their classification as CO 3.0–3.1 chondrites. These samples were tentatively paired during preliminary classification on the basis of geographic proximity of their find locations and petrographic similarity, but some differences have been observed in later studies. In addition to differences in bulk carbon isotopic compositions (Alexander et al. 2014), analyses of olivine in DOM 08006 indicate a grade of 3.0 but data for DOM 08004 indicate a grade closer to 3.1 (Fig. 11). Additional work, such as high-resolution matrix studies and determination of terrestrial ages, is needed for a fuller evaluation of whether or not these samples should be paired.

The CAI populations in the DOM samples have general similarities to each other and to those of previously described CO chondrites (e.g., Russell et al. 1998), so classification of both of them as COs is justified, though some COs have grossite-bearing CAIs and others do not. Greenwood et al. (1993) described a melilite-hibonite-grossite inclusion from Vigarano (CV3) in which grossite was the only phase altered, and they inferred that grossite is relatively highly susceptible to secondary alteration compared to other refractory phases. If grossite is easily destroyed, that could account for the incipient alteration seen in DOM 08004 grossite in the absence of other secondary phases, as in the Greenwood et al. (1993) case, and it would explain the difference in grossite contents between CO3.0–3.1 chondrites and higher-grade members. Differences between pristine chondrites, such as the presence (DOM) or absence (ALHA77307) of grossite-bearing inclusions, however, reflect true differences in the populations. Perhaps an Acfer 094-like subgroup of CO3 chondrites, with FeO-enriched and grossite-bearing CAIs, should be recognized, with DOM 08004 and 08006 as members. If such a group can be defined, it would help us understand the CO3s, and at last Acfer 094 would be placed in context with other meteorites.

SUMMARY AND CONCLUSIONS

There are some differences and some similarities between the DOM samples, Acfer 094, and ALHA77307. Although both DOM 08004 and DOM 08006 have been classified as CO3 chondrites, this work shows that they have stronger similarities to the ungrouped Acfer 094 than to the CO3 ALHA77307. Like Acfer 094, ~10% of the CAIs in the DOM samples are grossite-bearing; many phases in the refractory inclusions have elevated FeO contents compared to what would be expected to be found in typical, unaltered refractory inclusions; CAIs are small; and many inclusions have thin rims of melilite and/or aluminous diopside. In contrast, no grossite-bearing inclusions were found in ALHA77307; its melilite tends to have lower FeO contents than that in DOM samples or Acfer 094; fewer inclusions are enclosed in rim layers; and inclusions with melilite rims are very rare compared to the other samples considered here.

The primary phases in refractory inclusions in DOM 08004 and 08006 have FeO contents similar to those of their counterparts in Acfer 094, despite, like Acfer 094, having undergone little or no parent-body alteration. From their analyses and the lack of in situ alteration, Simon and Grossman (2011) concluded that the Acfer inclusions were exposed to an oxidizing, FeO-rich environment on another parent body prior to incorporation into the Acfer 094 parent body. A similar history is indicated for the inclusions in DOM 08004 and DOM 08006. These three meteorites might be best classified as a subgroup of CO3 chondrites, characterized by grossite-bearing refractory inclusions and inclusions with unusually high FeO contents in their refractory phases. Study of other CO chondrites of grades 3.0–3.1 might reveal additional members and help define the group.

Acknowledgments—We thank T. Fagan, J. Han, an anonymous reviewer, and A. Brearley (AE) for helpful comments. We thank the Meteorite Working Group for allocation of the thin sections of DOM 08004 and DOM 08006, and Dr. A. Davis for access to the thin section of ALHA77307 allocated to him. J. Davidson and R. Greenwood are thanked for providing helpful information. This work was supported by NASA grant NNX13AE73G (L. Grossman, PI) and funding is gratefully acknowledged.

Editorial Handling—Dr. Adrian Brearley

REFERENCES

Alexander C. M. O'D., Bowden R., and Howard K. T. 2014. A multi-technique search for the most primitive CO chondrites (abstract #2667). 45th Lunar and Planetary Science Conference. CD-ROM.

Brearley A. J. 1993. Matrix and fine-grained rims in the unequilibrated CO3 chondrite, ALHA77307: Origins and evidence for diverse, primitive nebular dust components. *Geochimica et Cosmochimica Acta* 57:1521–1550.

Brunner C. E. and Brearley A. J. 2011. TEM study of matrix in the CO3 chondrite ALHA77307: Clues about the first stages of metamorphism in chondrites (abstract #5403). 74th Annual Meeting of the Meteoritical Society. *Meteoritics & Planetary Science* 46:A31.

Cuvillier P., Leroux H., and Jacob D. 2014a. Fe-Mg zoning in forsterite in the Acfer 094 matrix: Evidence for a pre-accretionary interdiffusion process (abstract #5218). 77th Annual Meteoritical Society Meeting. *Meteoritics & Planetary Science* 49:A88.

Cuvillier P., Leroux H., and Jacob D. 2014b. Fe-Mg interdiffusion profiles in isolated forsterites in the Allende matrix. Evidence for a parent body origin: Time-temperature constraints deduced from a TEM study (abstract #1708). 45th Lunar and Planetary Science Conference. CD-ROM.

Davidson J., Busemann H., Alexander C. M. O'D., Nittler L. R., Hoppe P., Franchi I. A., and Grady M. M. 2008. Were presolar grains destroyed by the nebular process responsible for the volatile element fractionation? (abstract #1184). 39th Lunar and Planetary Science Conference. CD-ROM.

Davidson J., Busemann H., Alexander C. M. O'D., Nittler L. R., Schrader D. L., Orthous-Daunay F. R., Quirico E., Franchi I. A., and Grady M. M. 2009. Presolar SiC abundances in primitive meteorites by NanoSIMS raster ion imaging of insoluble organic matter (abstract #1853). 40th Lunar and Planetary Science Conference. CD-ROM.

Davidson J., Nittler L. R., Alexander C. M. O'D., and Stroud R. M. 2014. Petrography of very primitive CO3 chondrites: Dominion Range 08006, Miller Range 07687, and four others (abstract #1384). 45th Lunar and Planetary Science Conference. CD-ROM.

Davis A. M. 1985. Refractory inclusions in the Ornans C3O chondrite. Proceedings, 16th Lunar and Planetary Science Conference. pp. 165–166.

Floss C. and Stadermann F. J. 2012. Presolar silicate and oxide abundances and compositions in the ungrouped carbonaceous chondrite Adelaide and the K chondrite Kakangari: The effects of secondary processing. *Meteoritics & Planetary Science* 47:992–1009.

Greenwood R. C., Hutchison R., Huss G. R., and Hutcheon I. D. 1992. CAIs in CO3 meteorites: Parent body or nebula alteration? (abstract). *Meteoritics* 27:229.

Greenwood R. C., Morse A., and Long J. V. P. 1993. Petrography, mineralogy and Mg isotopic composition of VICTA: A Vigarano $CaAl_4O_7$-bearing Type A inclusion. Proceedings, 24th Lunar and Planetary Science Confernce. pp. 573–574.

Greshake A. 1997. The primitive matrix components of the unique carbonaceous chondrite Acfer 094: A TEM study. *Geochimica et Cosmochimica Acta* 61:437–452.

Grossman J. N. and Brearley A. J. 2005. The onset of metamorphism in ordinary and carbonaceous chondrites. *Meteoritics & Planetary Science* 40:87–122.

Grossman L. 2010. Vapor-condensed phase processes in the early solar system. *Meteoritics & Planetary Science* 45:7–20.

Han J. 2014. Microstructural constraints on the formational and thermal histories of refractory inclusions in CO3 chondrites. Ph.D. dissertation, University of New Mexico, Albuquerque, New Mexico, USA. 371 p.

Ireland T. R. 1990. Presolar isotopic and chemical signatures in hibonite-bearing refractory inclusions from the Murchison carbonaceous chondrite. *Geochimica et Cosmochimica Acta* 54:3219–3237.

Kimura M., El Goresy A., Palme H., and Zinner E. 1993. Ca-, Al-rich inclusions in the unique chondrite ALH 85085: Petrology, chemistry, and isotopic compositions. *Geochimica et Cosmochimica Acta* 57:2329–2359.

Kimura M., Grossman J. N., and Weisberg M. K. 2008. Fe-Ni metal in primitive chondrites: Indicators of classification and metamorphic conditions for ordinary and CO chondrites. *Meteoritics & Planetary Science* 43:1161–1177.

Kojima T., Yada S., and Tomeoka K. 1995. Ca-Al-rich inclusions in three Antarctic CO3 chondrites, Yamato-81020, Yamato-82050 and Yamato-790992: Record of low-temperature alteration. *Proceedings of the NIPR Symposium on Antarctic Meteorites* 8:79–96.

Krot A. N., Fagan T. J., Keil K., McKeegan K. D., Sahijpal S., Hutcheon I. D., Petaev M. I., and Yurimoto H. 2004. Ca, Al-rich inclusions, amoeboid olivine aggregates, and Al-rich chondrules from the unique carbonaceous chondrite Acfer 094: I. Mineralogy and petrology. *Geochimica et Cosmochimica Acta* 68:2167–2184.

Krot A. N., McKeegan K. D., Huss G. R., Liffman K., Sahijpal S., Hutcheon I. D., Srinivasan G., Bischoff A., and Keil K. 2006. Aluminum-magnesium and oxygen isotope study of relict Ca-Al-rich inclusions in chondrules. *The Astrophysical Journal* 639:1227–1237.

Ma C. and Rossman G. R. 2009. Davisite, $CaScAlSiO_6$, a new pyroxene from the Allende meteorite. *American Mineralogist* 94:845–848.

Ma C., Krot A. N., Nagashima K., and Tschauner O. 2014. Discovery of a new scandium aluminate mineral, $Ca_2Sc_6Al_6O_{20}$: An ultra-refractory phase in refractory inclusions from Murchison and Vigarano (abstract #1196). 45th Lunar and Planetary Science Conference. CD-ROM.

MacPherson G. J. and Grossman L. 1984. "Fluffy" type A Ca-, Al-rich inclusions in the Allende meteorite. *Geochimica et Cosmochimica Acta* 48:29–46.

MacPherson G. J., Bar-Matthews M., Tanaka T., Olsen E., and Grossman L. 1983. Refractory inclusions in the Murchison meteorite. *Geochimica et Cosmochimica Acta* 47:823–839.

Mason B. and Martin P. M. 1977. Geochemical differences among components of the Allende meteorite. *Smithsonian Contributions to the Earth Sciences* 19:84–95.

Nguyen A. N., Stadermann F. J., Zinner E., Stroud R. M., Alexander C. M. O'D., and Nittler L. R. 2007. Characterization of presolar silicate and oxide grains in primitive carbonaceous chondrites. *The Astrophysical Journal* 656:1223–1240.

Nguyen A. N., Nittler L. R., Stadermann F. J., Stroud R. M., and Alexander C. M. O'D. 2010. Coordinated analyses of

presolar grains in the Allan Hills 77307 and Queen Elizabeth Range 99177 meteorites. *The Astrophysical Journal* 719:166–189.

Nittler L. R., Alexander C. M. O'D., and Stroud R. M. 2013. High abundance of presolar materials in CO3 chondrite Dominion Range 08006 (abstract #2367). 44th Lunar and Planetary Science Conference. CD-ROM.

Pouchou J. L. and Pichoir F. 1984. A new model for quantitative X-ray microanalysis. Part I: Application to the analysis of homogeneous samples. *La Recherche Aerospatiale* 3:13–38.

Russell S. S., Huss G. R., Fahey A. J., Greenwood R. C., Hutchison R., and Wasserburg G. J. 1998. An isotopic and petrologic study of calcium-aluminum-rich inclusions from CO3 meteorites. *Geochimica et Cosmochimica Acta* 62:689–714.

Simon S. B. and Grossman L. 2011. Refractory inclusions in the unique carbonaceous chondrite Acfer 094. *Meteoritics & Planetary Science* 46:1197–1216.

Simon S. B. and Grossman L. 2014. Pristine chondrites DOM 08004 and DOM 08006: Grossite-rich CO3.0s or relatives of Acfer 094? (abstract #5177). 77th Annual Meteoritical Society Meeting. *Meteoritics & Planetary Science* 49:A364.

Simon S. B., Davis A. M., Grossman L., and Zinner E. K. 1998. Origin of hibonite-pyroxene spherules found in carbonaceous chondrites. *Meteoritics & Planetary Science* 33:411–424.

Simon S. B., Davis A. M., and Grossman L. 1999. Origin of compact type A inclusions from CV3 carbonaceous chondrites. *Geochimica et Cosmochimica Acta* 63:1233–1248.

Stroud R. M., Nittler L. R., and Alexander C. M. O'D. 2013. Analytical electron microscopy of a CAI-like presolar grain and associated fine-grained matrix materials in the Dominion Range 08006 CO3 meteorite (abstract #2315). 44th Lunar and Planetary Science Conference. CD-ROM.

Tomeoka K., Nomura K., and Takeda H. 1992. Na-bearing Ca-Al-rich inclusions in the Yamato-791717 CO carbonaceous chondrite. *Meteoritics* 27:136–143.

Vollmer C., Hoppe P., Stadermann F. J., Floss C., and Brenker F. E. 2009. NanoSIMS analysis and Auger electron spectroscopy of silicate and oxide stardust from the carbonaceous chondrite Acfer 094. *Geochimica et Cosmochimica Acta* 73:7127–7149.

Weber D. and Bischoff A. 1994. The occurrence of grossite ($CaAl_4O_7$) in chondrites. *Geochimica et Cosmochimica Acta* 58:3855–3877.